Brain Structure and Function (2020) 225:427–439
https://doi.org/10.1007/s00429-019-02017-1

ORIGINAL ARTICLE

Diffusion magnetic resonance imaging-derived free water detects neurodegenerative pattern induced by interferon-γ

Marcelo Febo[1,2,5,6] · Pablo D. Perez[1] · Carolina Ceballos-Diaz[2,3] · Luis M. Colon-Perez[1] · Huadong Zeng[5] · Edward Ofori[4] · Todd E. Golde[2,3,6] · David E. Vaillancourt[4,5,6] · Paramita Chakrabarty[2,3,6]

Received: 8 June 2019 / Accepted: 17 December 2019 / Published online: 1 January 2020

Abstract

Imaging biomarkers for immune activation may be valuable for early-stage detection, therapeutic testing, and research on neurodegenerative conditions. In the present study, we determined whether diffusion magnetic resonance imaging-derived free water signal is a sensitive marker for neuroinflammatory effects of interferon-gamma (Ifn-γ). Neonatal wild-type mice were injected in the cerebral ventricles with recombinant adeno-associated viruses expressing the inflammatory cytokine Ifn-γ. Groups of mice expressing Ifn-γ and age-matched controls were imaged at 1, 5 and 8 months. Mice deficient in Ifngr1$^{-/-}$ and Stat1$^{-/-}$ were scanned at 5 months as controls for the signaling cascades activated by Ifn-γ. The results indicate that Ifn-γ affected fractional anisotropy (FA), mean diffusivity (MD), and free water (FW) in white matter structures, midline cortical areas, and medial thalamic areas. In these structures, FA and MD decreased progressively from 1 to 8 months of age, while FW increased significantly. The observed reductions in FA and MD and increased FW with elevated brain Ifn-γ was not observed in *Ifngr1*$^{-/-}$ or *Stat1*$^{-/-}$ mice. These results suggest that the observed microstructure changes involve the Ifn-gr1 and Stat1 signaling. Interestingly, increases in FW were observed in midbrain of *Ifngr1*$^{-/-}$ mice, which suggests alternative Ifn-γ signaling in midbrain. Although initial evidence is offered in relation to the sensitivity of the FW signal to neurodegenerative and/or inflammatory patterns specific to Ifn-γ, further research is needed to determine applicability and specificity across animal models of neuroinflammatory and degenerative disorders.

Keywords Interferon gamma · Diffusion MRI · Free water · White matter · Aging · Inflammation

Introduction

Neurodegenerative diseases are characterized by a non-reversible loss of neurons, which significantly contributes to a range of adverse effects such as impaired cognition and vital sensorimotor functions. Characterization of in vivo biomarkers that can measure biological mechanisms involved in the initial stages of a neurodegenerative disease, particularly in relation to disease onset, is thus critical to developing effective and timely therapeutic interventions. For instance, there is growing evidence that aberrant brain immune activity precedes neurodegeneration in its earliest stages (Saxena and Caroni 2011). Therefore, biomarkers for such pathogenic immune responses may be valuable for early stage detection and intervention. Inflammatory immune activation is thought to form part of a temporally definable sequence of early events contributing to later neurodegeneration (Schwartz and Deczkowska 2016; Wyss-Coray 2016). Given the interplay between early inflammatory signaling proteins

✉ Marcelo Febo
febo@ufl.edu

1 Department of Psychiatry, College of Medicine, University of Florida, Gainesville, USA

2 Department of Neuroscience, College of Medicine, University of Florida, Gainesville, USA

3 Center for Translational Research in Neurodegenerative Diseases, College of Medicine, University of Florida, Gainesville, USA

4 Department of Applied Physiology and Kinesiology, College of Health and Human Performance, University of Florida, Gainesville, USA

5 Advanced Magnetic Resonance Imaging and Spectroscopy (AMRIS) Facility, College of Medicine, University of Florida, Gainesville, USA

6 McKnight Brain Institute, College of Medicine, University of Florida, Gainesville, USA

such as interferon-γ (Chakrabarty et al. 2011; Castano et al. 2002; Liscovitch and French 2014) in the pathological loss of neurons, a critical avenue towards developing early in vivo biomarkers of progression and increasing diagnostic precision is the characterization of preclinical methods that capture the deleterious effects of pathogenic immune signaling involved in neurodegenerative disorders.

Magnetic resonance imaging (MRI) provides a safe and relatively non-invasive means of revealing detailed age-progressive anatomical and functional changes, along with various morphometric measures of brain tissue microstructure (Febo and Foster 2016; Sahara et al. 2014; Colon-Perez et al. 2019). Measurement of these aspects of brain structure and function is vital when considering the limited access to pre-prodromal patient brain tissue for direct assessments. The translational strengths of diffusion MRI (dMRI) have provided a platform for in vivo testing of disease-specific hypotheses in animal models of neurodegenerative diseases (Sahara et al. 2014; Khairnar et al. 2015; Boska et al. 2007; Colon-Perez et al. 2019). However, the indirect nature of widely used proton-based MRI measurements limits measures of immune substrates and leads to uncertainties with regards to underlying biological factors when determining the impact of aberrant immune responses on brain microstructure and function. To this end, there have been significant advances in the modeling of tissue microstructure based on the differential displacement of molecular water in restricted intracellular spaces and hindered extracellular environments and in more freely diffusing tissues such as cerebrospinal fluid (CSF) (Assaf and Basser 2005; Pasternak et al. 2012). The free water index, which attempts to quantify relative fraction of freely diffusing water in the extracellular space, is thought to be affected by neurodegenerative and neuroinflammatory processes (Ofori et al. 2015b, 2017; Pasternak et al. 2014, 2016, 2012; DeSimone et al. 2017; Burciu et al. 2017). Despite the promise of such dMRI analysis methods, the degree to which neuroinflammation and neurodegeneration affects the previously reported free water index (Ofori et al. 2015b, 2017; Pasternak et al. 2014, 2016, 2012; DeSimone et al. 2017; Burciu et al. 2017) is still poorly understood.

In the present study, we used genetic tools coupled with high-field dMRI to determine microstructural changes associated with inflammation and neurodegeneration in the brains of mice induced to overexpress the inflammatory cytokine interferon-γ (Ifn-γ). We previously showed that recombinant AAV(rAAV)-mediated expression of mouse Ifn-γ in wildtype (WT) mice induces progressive nigrostriatal degeneration and midbrain calcinosis (Chakrabarty et al. 2011) in a manner that recapitulates neurodegenerative diseases such as atypical Parkinsonism (Strickland et al. 2017). We report here that the free water signal and to a lesser degree fractional anisotropy (FA) and mean diffusivity (MD) are sensitive to age-progressive neuropathological changes in the AAV-Ifn-γ mouse model. Furthermore, using mice ($Ifngr1^{-/-}$ and $Stat1^{-/-}$) that are genetically deficient of Ifn-γ signaling proteins (Huang et al. 1993; Durbin et al. 1996), we demonstrate that the measured Ifn-γ-induced free water alterations are partially linked to a canonical Ifn-γ signaling pathway (Strickland et al. 2017). Thus, the Ifn-γ receptor *Ifngr1* or its intracellular signaling protein *Stat1* were shown here to be important contributors to the observe Ifn-γ-induced alterations in the free water index induced in cortex, white matter, and thalamus of aged mice.

Methods

Mice

Mice were housed in groups of 3–4 in conventional cages (29 × 18 × 13 cm) at 20–26 °C (lights on from 0700 to 1900 h) with food and water ad libitum. Wildtype (WT) B6/C3H mice were obtained from Envigo (Indianapolis, Indiana), $Ifngr1^{-/-}$ mice (129-Ifngr1tm1Agt/J) from Jackson Labs (Bar Harbor, Maine) and $Stat1^{-/-}$ mice from the laboratory of Joan Durbin, PhD (New York University School of Medicine). $Ifngr1^{-/-}$ and $Stat1^{-/-}$ mice strains were maintained as homozygotes, originally derived on the B6/C3H genetic background. WT mice were imaged at 1, 5 and 8 months ($n = 32$ mice total, $n = 4$–6 mice/age/treatment), whereas $Ifngr1^{-/-}$ ($n = 10$ mice/age/treatment) or $Stat1^{-/-}$ ($n = 7$ mice/age/treatment) were imaged at 5 months of age. All groups were gender and age matched. All procedures received prior approval from the Institutional Animal Care and Use Committee of the University of Florida and follow all applicable NIH guidelines.

Adeno-associated viral vector (AAV) preparation and brain delivery

Murine Ifn-γ (mIFN-γ) and enhanced green fluorescent protein (EGFP) were packaged in AAV capsid 1 and injected on neonatal day P2 as previously reported (Ayers et al. 2015). Details of these methods and the animal model have been recently reported (Strickland et al. 2017). AAV-EGFP served as control for AAV-Ifn-γ.

Diffusion magnetic resonance imaging

Images were acquired using an 11.1 Tesla MRI scanner (Magnex Scientific Ltd., Oxford, UK) with an Agilent 205/120HD gradient set (maximum gradient strength 600mT/m and rise time of 130 μs) controlled by VnmrJ 3.1 console software, as previously reported (Sahara et al. 2014). An in-house 2.0 × 2.5 cm quadrature surface transmit/receive

coil tuned to 470.7 MHz (^{1}H resonance) was used for B1 excitation and signal detection (AMRIS Facility, Gainesville, FL). Anesthesia was initially induced under 2.0–2.5% isoflurane (0.1–0.15 L/min) delivered in 100% oxygen for 30–60 s. Isoflurane levels were then maintained between 1.0 and 1.25% throughout the entire setup and imaging session to maintain stable respiration rates. Mice were placed prone on a custom-made plastic bed with a respiratory pad placed underneath the abdomen. Respiratory rates were monitored continuously and maintained between 25–40 beats per minute by adjusting isoflurane levels. Core body temperature was maintained at 37–38 °C using a warm water recirculation system (SA Instruments, Inc., New York).

A multi-slice gradient echo sequence with the following parameters was used as an anatomical reference scan: $256^2 \times 6$ sagittal slices covering midline brain structures, field of view (FOV) 25 mm$^2 \times 0.75$ mm slice thickness (in plane resolution 97 μm^2), flip angle = 20°, 8 averages, echo time (TE) = 3.8 ms and repetition time (TR) = 100 ms. Initial test scans in control and Ifn-γ showed significant signal loss and distortion in lateral/temporal cortical regions near the ear canal of mice, when acquiring coronal brain slices using an in-house-built mouse quadrature transmit/receive coil. Thus, we used a sagittal slice orientation which omitted these lateral regions and allowed us to cover most of the midline cortical, thalamic, basal ganglia, and white matter structures previously investigated in the Ifn-γ mouse model (Chakrabarty et al. 2011; Strickland et al. 2017). Diffusion weighted scans were acquired using a 4-shot spin echo planar imaging (EPI) sequence with TR = 2000 ms, TE = 38 ms, gradient amplitude of 18.47 G/cm, gradient duration $\delta = 6$ ms, diffusion time $\Delta = 12$ ms, maximum b value of 900 s/mm^2, and 42 gradient directions (icosahedral shaped sampling scheme) with six additional B0 images interleaved between every seven diffusion-sensitized images. Diffusion images had the same FOV and slice thickness as the anatomical reference scan but with a lower resolution data matrix size of 128^2 and 6 slices at 0.75 mm each (in plane resolution, 195 μm^2; in the same space as anatomical scans to facilitate anatomical alignment to an MRI atlas of the mouse brain).

Image postprocessing

Diffusion MRI scans were processed using tools available on FMRIB software library—FSL (Smith et al. 2004), as previously reported for mouse dMRI scans obtained at 11.1 Tesla (Sahara et al. 2014). FSL EDDY_CORRECT program was used for affine registration of diffusion weighted images to the first B0. Gradient vectors were rotated according to the resulting motion correction vectors.

We used the free water elimination algorithm to estimate the fractional contribution of freely diffusing, hindered water present in the extracellular space to the overall diffusion signal per voxel (Pasternak et al. 2012). There is evidence that such an approach enhances the accuracy of diffusivity and anisotropy measurements (Pasternak et al. 2012). Diffusion datasets were processed first by carrying out a voxel-wise fitting procedure in MATLAB (Natick, MA) using a two-compartment model of diffusion that includes terms for tissue and extracellular free water diffusivity (Pasternak et al. 2009, 2012; DeSimone et al. 2016). This step produced a mouse brain image of free water (indexed from 0 to 1, the latter meaning highest extracellular free water) and a diffusion tensor with free water fraction removed (free water corrected tensor, or FW). The corrected tensor was processed using DTIFIT on FSL to produce maps of FA and MD (called here 'corrected' FA_c or MD_c) (Behrens et al. 2003).

To investigate differences in FW, FA_c or MD_c between WT mice with and without Ifn-γ expression, we conducted whole brain statistical analyses on scalar maps and also region of interest (ROI)-based analyses in MATLAB (see following section). To do this, we first used FSL FLIRT software to align anatomical scans for each subject to a composite reference template (higher resolution T2-weighted fast spin echo scan) used in the creation of a fully segmented atlas of the mouse brain (Ferris et al. 2014). Prior to subject to template registration, binary masks outlining the mouse brain on the anatomical scans were manually generated using ITKSNAP (Yushkevich et al. 2006). The binary 'brain-only' masks were multiplied by anatomical scans to null voxels outside the brain. The cropped anatomical brain images were then aligned to a mouse brain template using 12-parameter affine registration, a full 180° search, and a correlation ratio search cost in FLIRT (Jenkinson et al. 2002) (Fig. 1a). Registration matrices for each subject were saved and used to transform post-processed scalar maps (FW, FA_c and MD_c) to the template space for analysis.

Statistical analysis

Whole brain analyses were carried out in Analysis of Functional Neuroimages (AFNI) (Cox 1996) using two-factor Analysis of Variance (ANOVA: age [3 levels] × Ifn-γ treatment [2 levels]) computations available in three-dimensional multi-variate modeling (3dMVM) (Chen et al. 2014). The groups tested were the following: 1-month/control ($n = 4$), 5-month/control ($n = 4$), 8-month/control ($n = 6$), 1-month/ Ifn-γ ($n = 4$), 5-month/ Ifn-γ ($n = 4$), 8-month/ Ifn-γ ($n = 5$). In 3dMVM, four general linear tests were carried out, which created maps for main effect of age, main effect of treatment, age x treatment, and post hoc t tests comparing WT Ifn-g vs. WT controls. All maps for FW, FA_c, and MD_c were false discovery rate (FDR) corrected and thresholded at p values for $q < 1$ to 5%.

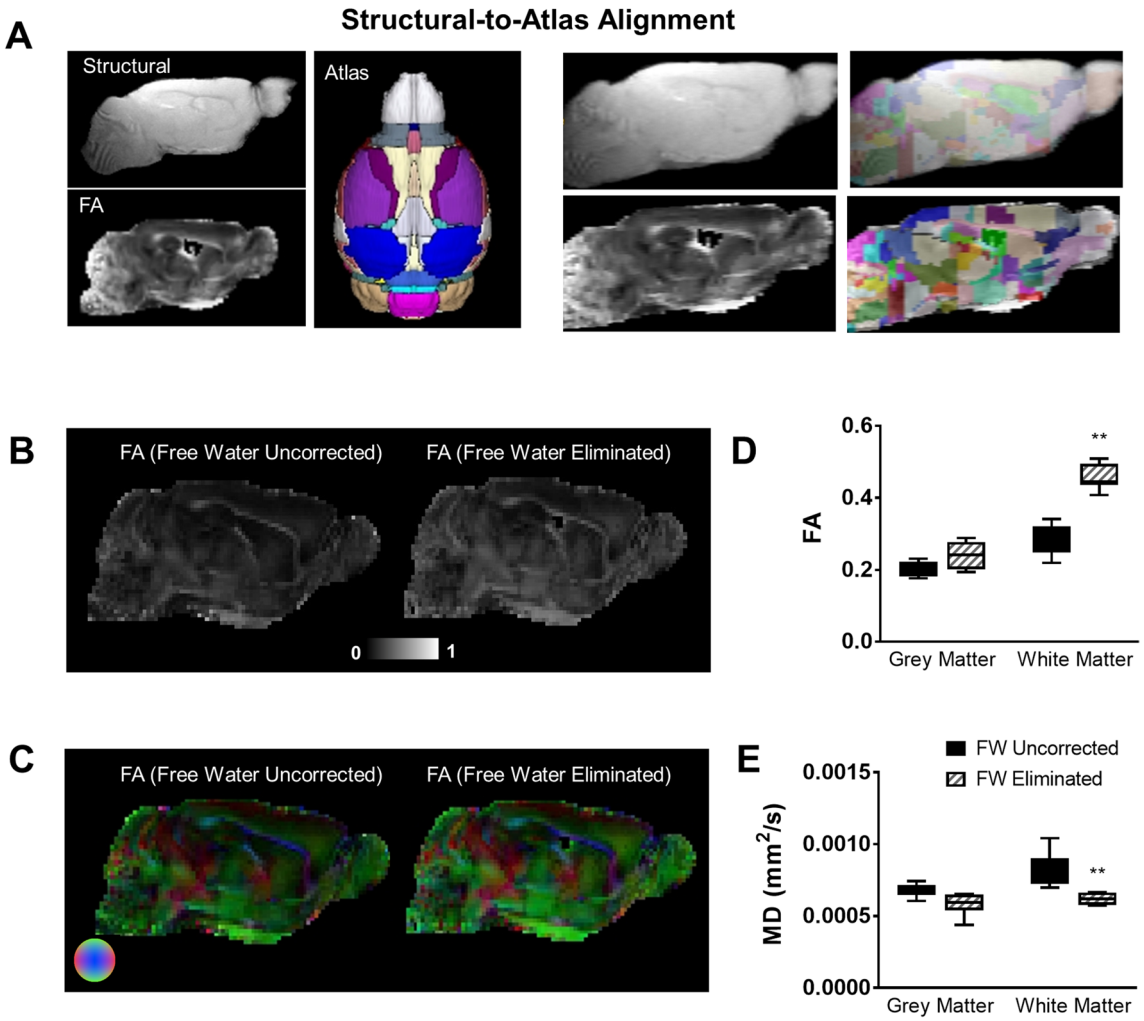

Fig. 1 Steps used in image preprocessing. **a** Alignment of anatomical scans to a structural reference scan and segmented atlas. **b** Comparison of fractional anisotropy images, before and after free water elimination. **c** FA maps with color encoded directionality (sphere with red green blue indicates direction). **d** FA and **e** mean diffusivity values (mm^2/s) for grey matter (frontal cortex) and white matter (corpus callosum) of eight control WT mice. Data presented as Tukey box and whisker plots (median, 25–75th percentile and 1.5 interquartile range). **Significantly different from uncorrected values (Tukey's post hoc test)

For ROI analyses, FW, FA_c, and MD_c values per each ROI were exported in spreadsheet form and imported into MATLAB for analysis using two-way ANOVA and Tukey's post hoc test. Mean ROI data were extracted from each subjects' FW, FA_c, and MD_c scalar maps using ROI masks generated using the inverse of the subject-to-atlas registration matrices. Nineteen ROIs were included in the ANOVA comparisons. Family-wise error correction (Sidak's multiple comparison correction) was used and, therefore, significant differences were considered for $p \leq 0.003$.

Results

Elevated brain Ifn-γ is associated with age-progressive alterations in free water, fractional anisotropy and mean diffusivity

We investigated whether the free water signal can detect age-progressive alterations that are consistent with previously reported neuroinflammatory and neurodegenerative

effects of Ifn-γ in WT mice (Strickland et al. 2017; Chakrabarty et al. 2011). These alterations include dystrophic calcification in the basal ganglia and a nigrostriatal degenerative phenotype (Strickland et al. 2017). A major prediction was that the free water index in the brain varied as a function inflammatory and neurodegenerative status resulting from brain-specific Ifn-γ overexpression. Although the free water elimination processing of dMRI scans did not induce any appreciable changes in FA or directionality maps (Fig. 1b, c), we confirmed that free water elimination adjusted FA and MD values in the mouse brain. Free water elimination increased white matter FA and reduced MD values relative to uncorrected diffusion scans (Fig. 1d, e; FA: $F_{1,28} = 79$ $p < 0.0001$; MD: $F_{1,28} = 26$ $p < 0.0001$). Grey matter measurements showed similar, albeit non-significant trends for FA and MD (Fig. 1d, e).

The anatomical scans of 5–8-month-old Ifn-γ WT mice showed highly consistent signs of pathology in the midbrain and thalamic areas, not present in WT controls of any age. This was present in all scans for these groups. The lesion-like dark areas are first noted in Ifn-γ wildtype (WT) mice at 3 months (not shown) and increases in severity by 5–8 months (mo) of age (Fig. 2a). Lesions similar to these are observed in radiographic images of patients with idiopathic basal ganglia calcification (IBGC) (Zaitout et al. 2014). In the calculated free water maps of Ifn-γ WT mice,

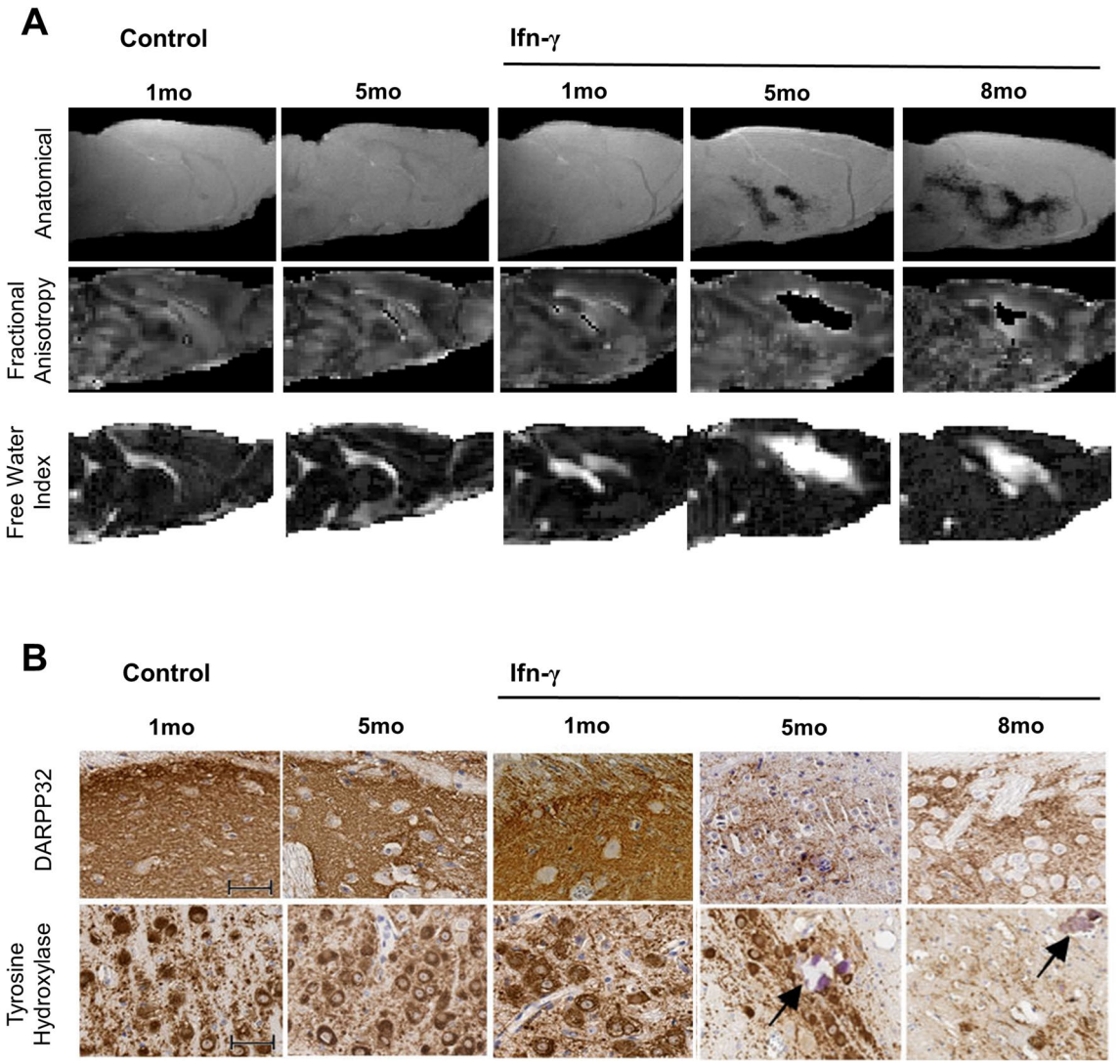

Fig. 2 Elevated Ifn-γ expression produces age-progressive increases in free water signal in brain regions with coincident reductions in fractional anisotropy and inflammation-induced lesions. **a** Representative structural, fractional anisotropy and free water maps of control mice and mice overexpressing Ifn-γ, shown at different ages. **b** Reduced nigral DARPP32 and Th immunostaining demonstrate age-progressive degeneration in the midbrain of Ifn-γ mice compared to control mice. Arrow in immunohistochemical panels denotes dystrophic calcinosis

we observed hyperintense areas corresponding to areas of increased volume of extracellular free water and these areas included and extended beyond CSF ventricular regions in Ifn-γ but not in control WT mice (Fig. 2a). The extent of the spreading of these hyperintense high free water regions is observed as early as 1 month of age in Ifn-γ mice (compared to age-matched control mice) and expands progressively with age (Fig. 2a). Consistent with previous histopathological assessments (Strickland et al. 2017), Ifn-γ mice showed significant age-progressive loss of dopaminergic neurons in substantia nigra pars compacta (Fig. 2b). Therefore, the pathological effects of Ifn-γ treatment are consistent with the previous two studies using this model.

For FA_c, ANOVA revealed a significant main effect of Ifn-γ treatment, but not of age, in the corpus callosum ($F_{1,21} = 17.6$, $p = 0.0004$) and fimbria ($F_{1,21} = 21.9$, $p = 0.0001$) (Figs. 3 and 4, top). In the corpus callosum, Tukey's post hoc test indicated a significantly greater FA_c in 8-month control vs 5- or 8-month Ifn-γ ($p < 0.05$). We also observed a significantly greater FA_c in 8-month Ifn-γ mice vs any WT control group and 1-month Ifn-γ ($p < 0.05$).

For FW, ANOVA revealed a significant age × Ifn-γ treatment interaction in the corpus callosum (Ifn-γ treatment: $F_{1,21} = 86.4$, $p < 0.00001$; age: $F_{2,21} = 9.1$, $p = 0.001$; interaction: $F_{2,21} = 7.9$, $p = 0.0027$), and significant main effect of Ifn-γ treatment in the cingulate gyrus ($F_{1,21} = 39.5$, $p < 0.00001$), fimbria ($F_{1,21} = 48.9$, $p < 0.00001$), rostral retrosplenial cortex ($F_{1,21} = 24.1$, $p = 0.0001$) and mediodorsal thalamus ($F_{1,21} = 14.5$, $p = 0.001$) (Figs. 3 and 4, middle). In the corpus callosum, Tukey's post hoc test indicated significantly greater FW values in 8-month WT mice treated with Ifn-γ relative to any WT control group and 1-month Ifn-γ mice ($p < 0.05$). In the cingulate cortex and mediodorsal thalamus, there was significantly greater FW values in 8-month Ifn-γ mice relative to any WT control group and 1-month Ifn-γ mice ($p < 0.05$). In fimbria and restrosplenium, there was significantly greater FW values in 8-month Ifn-γ relative to all other groups ($p < 0.05$).

For MD_c, ANOVA revealed a significant main effect of Ifn-γ treatment, but not of age, in the corpus callosum ($F_{1,21} = 14.0$, $p = 0.001$) and fimbria ($F_{1,21} = 17.8$, $p = 0.0004$) (Figs. 3 and 4, bottom). In both these white matter structures, Tukey's post hoc test indicated a significantly greater FA_c in 8-month control vs 5- or 8-month Ifn-γ ($p < 0.05$).

Ifn-γ receptor-1 or Stat1 signaling proteins are important in mediating the effects of Ifn-γ on free water, fractional anisotropy and mean diffusivity

It was recently reported that the pathogenic effects of Ifn-γ in WT mice are abrogated in mice lacking Ifngr1 or Stat1 (Strickland et al. 2017). In the present study, we wanted to further examine whether Ifngr1 and Stat1 are necessary for brain Ifn-γ expression to cause the above-mentioned alterations on the free water index, FA_c and MD_c (Fig. 5). First, the midbrain/thalamic hypointense areas observed in anatomical reference scans of 5-month and 8-month Ifn-γ mice were no longer observed in age-matched *Ifngr1*$^{-/-}$ or *Stat1*$^{-/-}$ mice induced to express Ifn-γ (Fig. 5). The lack of effect of Ifn-γ in producing these MR lesions is consistent with previous histopathological assessments indicating that neither *Ifngr1*$^{-/-}$ nor *Stat1*$^{-/-}$ mice develop any basal ganglia calcinosis in the presence of Ifn-γ (Strickland et al. 2017). Conversely, hyperintense areas on free water maps of Ifn-γ *Ifngr1*$^{-/-}$ or *Stat1*$^{-/-}$ mice were not distinct from 5-month WT control mice and much lower than in age-matched Ifn-γ mice (Fig. 5).

We analyzed the effect of Ifn-γ in *Ifngr1*$^{-/-}$ or *Stat1*$^{-/-}$ mice. We predicted that if in WT mice Ifn-γ produced changes in FW and other microstructure measures, these would be absent in mice lacking either the Ifn-γ receptor-1 or Stat1 signaling protein. Results are shown in Fig. 6. We conducted comparisons only between 5-month-old mice, which included WT controls, WT Ifn-γ, and *Ifngr1*$^{-/-}$ or *Stat1*$^{-/-}$ mice with elevated Ifn-γ. We used a one-way ANOVA with Ifn-γ vs control as the main factor.

For FA_c, ANOVA revealed a significant main effect of Ifn-γ treatment, but not of age, in fimbria ($F_{3,21} = 7.2$, $p = 0.002$) (Fig. 6, top). Tukey's post hoc test indicated a significantly reduced FA_c with Ifn-γ treatment in WT and in *Ifngr1*$^{-/-}$ mice relative to WT controls ($p < 0.05$).

For FW, ANOVA revealed a significant main effect of Ifn-γ treatment in anterior thalamic area ($F_{3,21} = 6.4$, $p = 0.003$), corpus callosum ($F_{3,21} = 52.1$, $p < 0.000001$), cingulate cortex ($F_{3,21} = 22.2$, $p < 0.00001$), fimbria ($F_{3,21} = 13.9$, $p = 0.00003$), substantia nigra ($F_{3,21} = 11.0$, $p = 0.0001$) and ventral tegmental area ($F_{3,21} = 8.4$, $p = 0.0007$) (Fig. 6, middle). With the exception of the two midbrain ROI's, these brain regions had an increased FW in WT mice expressing Ifn-γ and this was not observed in *Ifngr1*$^{-/-}$ or *Stat1*$^{-/-}$ mice. The Ifn-γ receptor-1 or Stat1 signaling protein may have been necessary for Ifn-γ to produce increases in FW. Thus, Tukey's post hoc test indicated that there were greater FW values in WT Ifn-γ compared to WT controls and *Ifngr1*$^{-/-}$ or *Stat1*$^{-/-}$ mice expressing Ifn-γ ($p < 0.05$). In the midbrain areas, we observed that while Ifn-γ did not increase FW values in WT mice, it did in *Ifngr1*$^{-/-}$ mice (Tukey's post hoc test $p < 0.05$ compared to WT control, WT Ifn-γ and *Stat1*$^{-/-}$ mice).

For MD_c, ANOVA revealed a significant main effect of Ifn-γ treatment in the hippocampal CA3 ($F_{3,21} = 6.6$, $p = 0.0026$), corpus callosum ($F_{3,21} = 7.9$, $p = 0.001$), and fimbria ($F_{3,21} = 9.6$, $p = 0.0003$). In these regions, Ifn-γ in WT mice, but not *Ifngr1*$^{-/-}$ or *Stat1*$^{-/-}$ mice, reduced MD values (Tukey's post hoc test, $p < 0.05$).

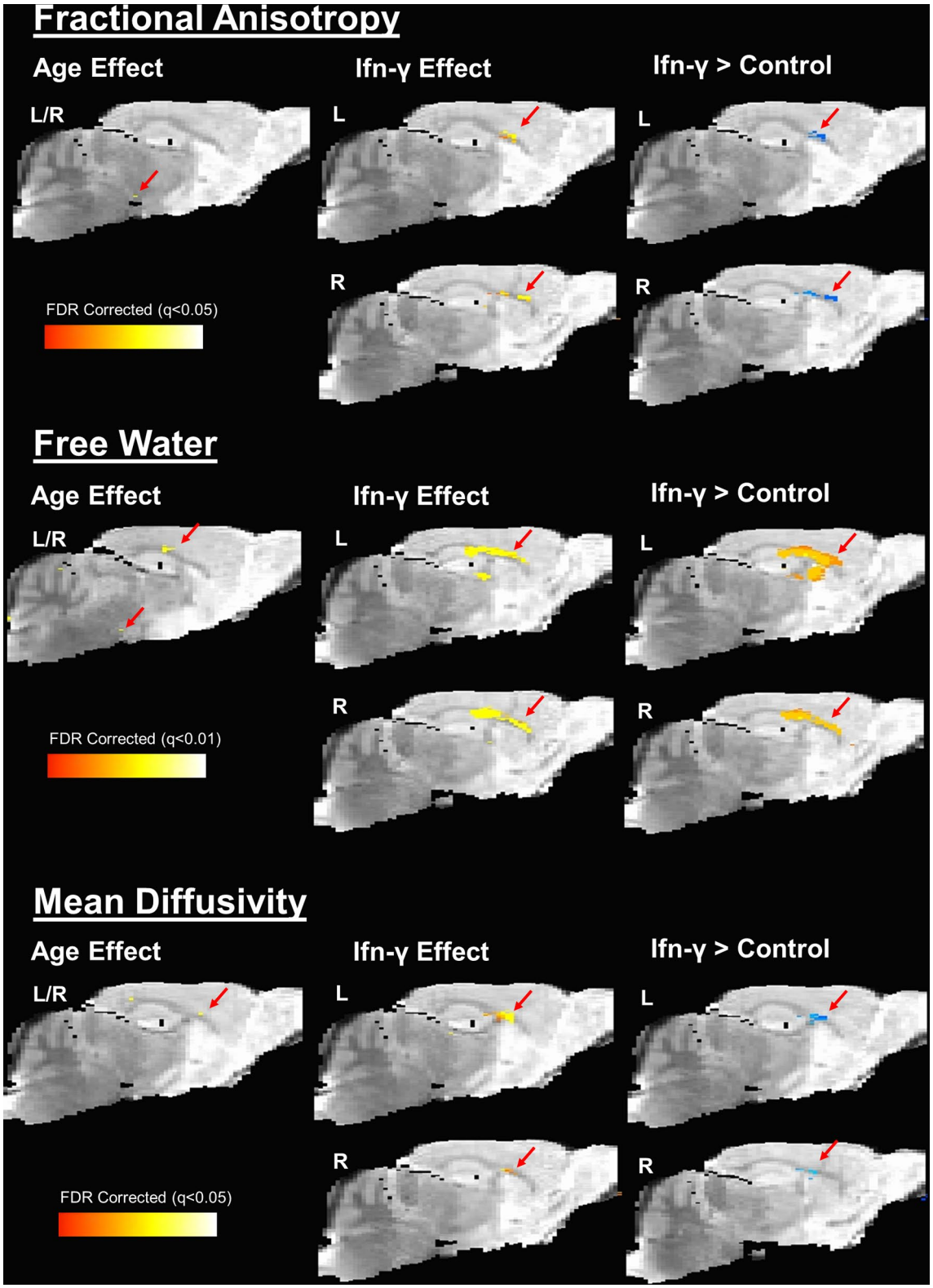

Fig. 3 Composite statistical maps indicate that Ifn-γ produced significant changes in fractional anisotropy (FA), free water (FW) and mean diffusivity (MD) in white matter and surrounding regions of the mouse brain. Shown are significant voxels in left (L) and right (R) hemispheres (arrows note significantly different voxels). All images are false discovery rate (FDR) corrected with a p value corresponding to a FDRq threshold ≤ 1–5%. Ifn-γ produced reductions in FA and MD and increases in FW relative to WT control mice

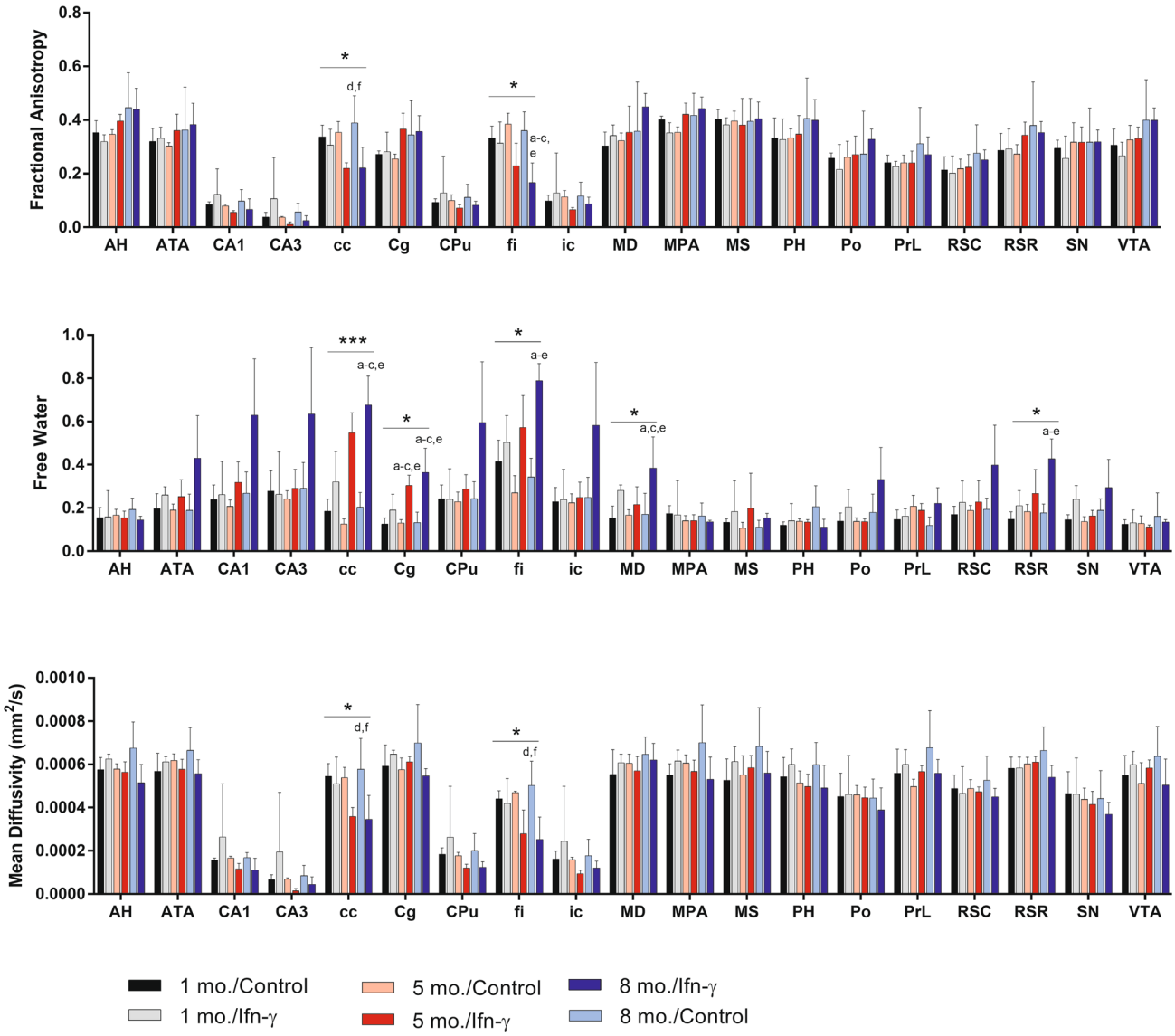

Fig. 4 Ifn-γ reduced fractional anisotropy and mean diffusivity and increased free water in white matter, midline cortical and thalamic areas. Two-factor ANOVA and Bonferroni post hoc multiple comparison test. *main effect of Ifn-γ treatment, **main effect of age, and ***treatment x age interaction (Bonferroni corrected $p < 0.003$; $n = 4$–5 mice/group). Error bars are standard deviation. Symbols above bars are significantly different from: a = 1-month control, b = 1-month Ifn-γ, c = 5-month control, d = 5-month Ifn-γ, e = 8-month control, f = 8-month Ifn-γ. *AH* anterior hypothalamus, *ATA* anterior thalamic area, *CA1/3* cornus Ammonis 1/3, *cc* corpus callosum, *CPu* caudate-putamen, *fi* fimbria, *ic* internal capsule, *MD* mediodorsal thalamus, *MPA* medial preoptic area, *MS* medial septum, *PH* posterior hypothalamus, *Po* posterior thalamus, *PrL* prelimbic cortex, *RSC/R* retrosplenial cortex-caudal/rostral, *SN* substantia nigra, *VTA* ventral tegmental area

Discussion

Using dMRI and the free water correction method (Ofori et al. 2015b; Pasternak et al. 2014, 2016, 2012; DeSimone et al. 2017), we show that free water index values are significantly elevated in white matter of 8-month AAV-Ifn-γ mice relative to controls or younger 1-month Ifn-γ cohorts. The effect of Ifn-γ is consistent with gliosis and neurodegenerative changes reported in a previous study using the same animal model (Chakrabarty et al. 2011; Strickland et al. 2017). Overall, our data support the notion that along with FA and MD values from dMRI scans, free water also provides a somewhat sensitive measure of microstructural changes previously reported to occur in the AAV-Ifn-γ mouse (Strickland et al. 2017). A significant finding of the present work are data demonstrating that in some brain areas, the free water index in Ifn-γ-overexpressing *Ifngr1*$^{-/-}$ mice and *Stat1*$^{-/-}$ mice are comparable to control

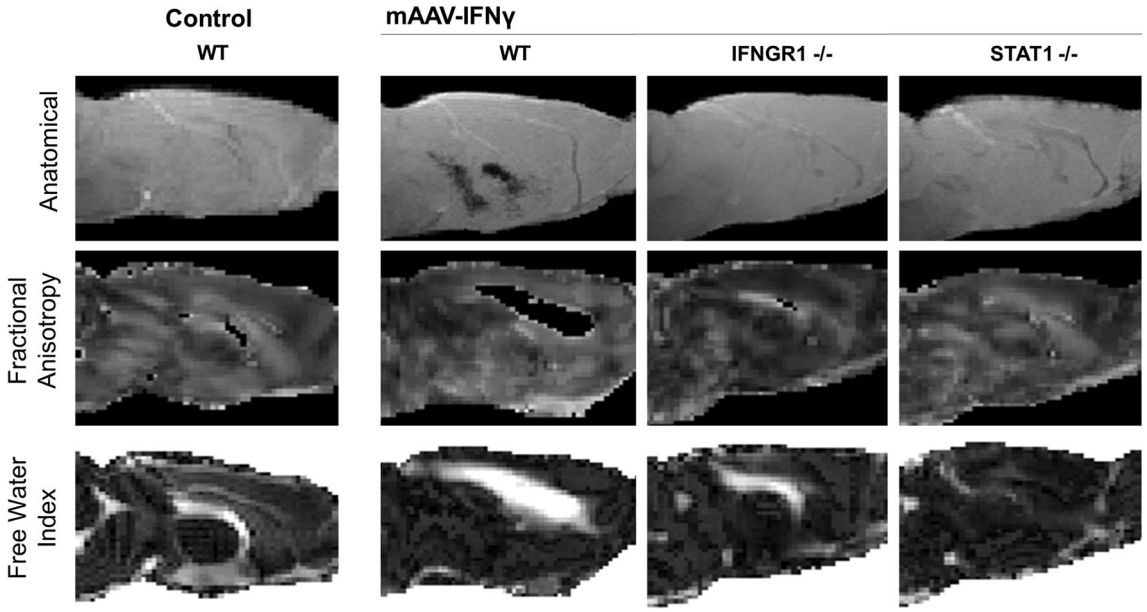

Fig. 5 Ifn-γ induced increases in free water, reduced fractional anisotropy, and inflammation-induced lesions are not observed in *Ifngr1* and *Stat1* null mice

mice, suggesting that Ifn-γ-induced free water changes entail a mechanistic link with this canonical inflammatory pathway. Furthermore, the observed effects of Ifn-γ in elevating the free water index in aged mice demonstrates a degree of specificity with regards to the necessary presence of *Ifngr1* and *Stat1* transignaling proteins. The results thus establish a novel link between this dMRI measure and inflammation in an animal model shown previously to sustain significant nigrostriatal neuronal loss (Strickland et al. 2017).

Pasternak et al (2012) were the first to show evidence that extracellular free water volume is a surrogate measure for neuroinflammation by distinguishing neurodegenerative axonal white matter changes from free water changes in grey and white matter regions in schizophrenics (Pasternak et al. 2012). This method has also been applied to research on white matter degeneration in Alzheimer's disease (AD), cerebrovascular disease contributions to dementia and in healthy aging (Maier-Hein et al. 2015; Albi et al. 2017; Hoy et al. 2017; Ji et al. 2017). Compared to non-cerebrovascular disease healthy controls, AD subjects had higher free water index values in white matter structures, which was worse in AD with cerebrovascular damage (Ji et al. 2017). The extent of cerebrovascular damage, white matter pathology and free water correlated with severity of cognitive impairment and this in turn was associated with pathological changes in frontal cortical and occipital lobe structures (Ji et al. 2017). Free water imaging has also been recently used in Parkinsonism to delineate how free water corrected dMRI signals track neuropathological alterations in a spectrum of patients with Parkinson's disease, multiple system atrophy, and progressive supranuclear palsy. Ofori and colleagues showed in two datasets of Parkinson's disease from multisite studies that free water increases specifically in the posterior substantia nigra in these patients with no differences observed in FA (Ofori et al. 2015a). Free water signal increases further in patients re-scanned a year after their first measurement, supporting the use of free water imaging as a biomarker for progression (Ofori et al. 2015a). A second study showed a similar trend in free water values in atypical Parkinsonian patients, although in this case, increased free water was also observed outside the posterior substantia nigra, a result similar to what we report here using a mouse model recapitulating aspects of atypical Parkinsonism (Strickland et al. 2017). The regions showing increased free water in these atypical patients included corpus callosum, cerebellum, caudate, putamen, and thalamus (Planetta et al. 2016). While the above-cited clinical studies indicate that changes in the free water index could be associated with cell loss, inflammation and/or cerebrovascular damage, direct causal links have not been investigated. The present study represents initial attempts to understand the underlying links between the free water index and inflammatory and neurodegenerative processes in a previously studied animal model (Strickland et al. 2017).

When expressing Ifn-γ in the absence of Stat1, we previously observed elevated signs of neuroinflammation (Strickland et al. 2017), which included increased astrogliosis. The observed neuroinflammatory state in Ifn-γ mice preceded and was thought to drive nigrostriatal cell loss (Strickland et al. 2017), a result consistent with our previous data

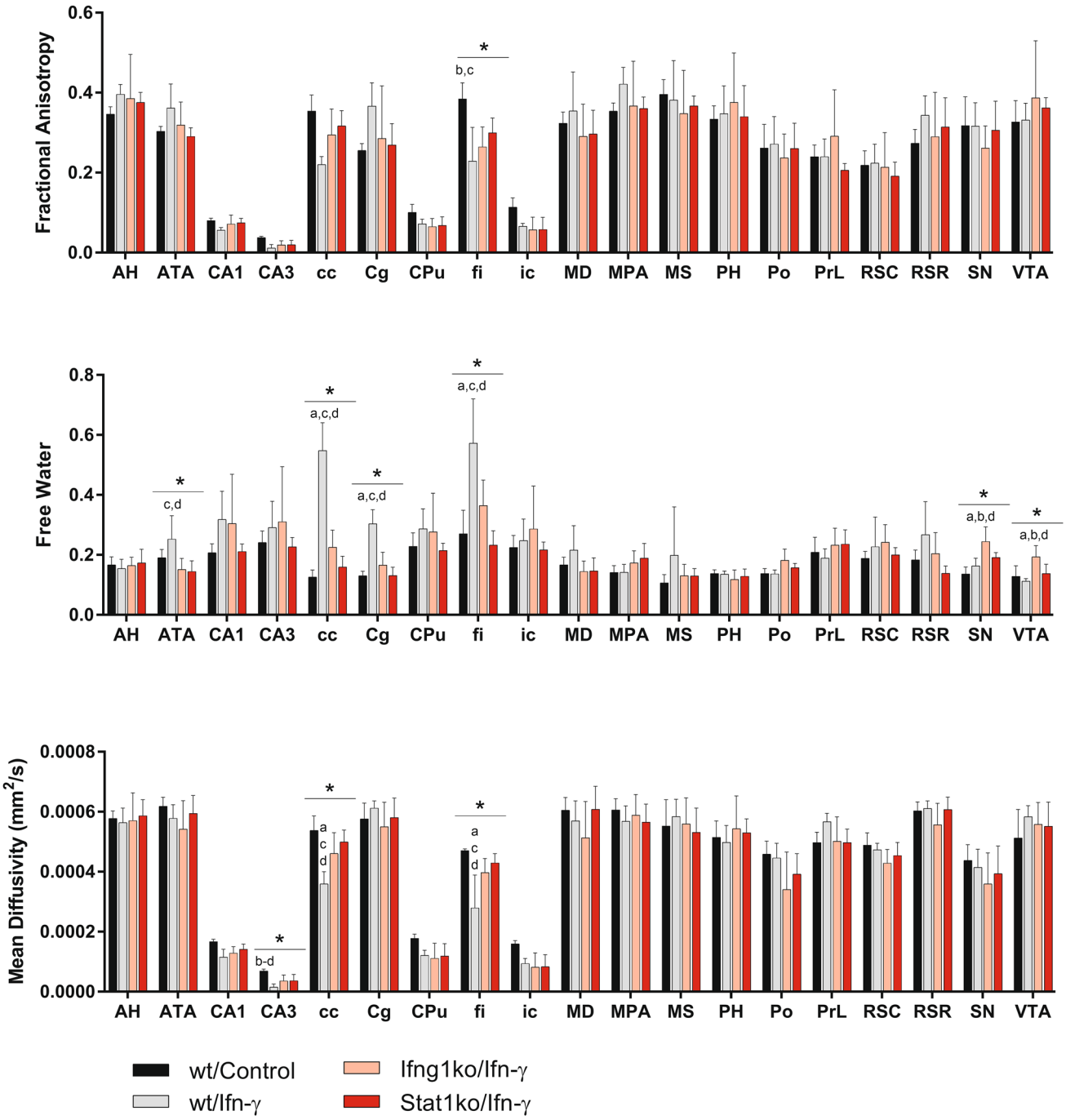

Fig. 6 Ifn-γ induced changes in fractional anisotropy, mean diffusivity and free water were largely absent in *Ifngr1*$^{-/-}$ and *Stat1*$^{-/-}$ mice. Two-factor ANOVA and Bonferroni post hoc multiple comparison test. *main effect of Ifn-γ treatment, **main effect of age, and ***treatment × age interaction (Bonferroni corrected $p < 0.003$; $n = 4$–10 mice/group). Error bars are standard deviation. Symbols above bars are as in Fig. 4. Abbreviations are as in Fig. 4

(Chakrabarty et al. 2011), as the nigro-striatal degenerative feature was not observed in Stat1-/- mice despite increased inflammation. Interestingly, in the current imaging study, we did not observe elevated free water index in the brain of *Stat1*$^{-/-}$ mice in spite of increased astrogliosis (Strickland et al. 2017). One possible explanation is that this index of free water is more sensitive to neurodegenerative processes than to inflammatory signaling-induced changes in activated glial cells. Future studies are needed to address this possibility by directly distinguishing between inflammatory state, in the presence or absence of neurodegeneration. Another possible explanation is that extracted free water

index values are only partially sensitive to one or a few of a broader range of brain immune cell inflammatory responses to Ifn-γ. Alternative in-depth dMRI microstructure models capturing more details or specificity of potential effects of underlying inflammation, cellular morphological alterations or cell loss might be more useful in this regard (Assaf and Basser 2005; Zhang et al. 2012).

We used an AAV-Ifn-γ mouse model to provide us with a mechanistic basis linking neuroinflammation, neurodegeneration, and a dMRI metric with potential clinical relevance. Initial examination of uncorrected FA and MD revealed changes consistent with the inflammatory or degenerative phenotypes in these mice. However, after free water correction, many of the observed changes in FA and MD were no longer significant and instead we observed that free water signal tracked changes in the brain that were consistent with previously reported Ifn-γ-induced astrogliosis (Strickland et al. 2017) and could thus serve as a measure of Ifn-γ-induced neuroinflammation or neurodegenerative pathology. This also suggests that careful consideration should be taken when interpreting FA/MD metrics from dMRI data and it also supports the use of alternate tissue microstructure methods that can provide a more detailed account of underlying geometric features of the tissue in health and disease (Metzler-Baddeley et al. 2012; Ofori et al. 2015a; Planetta et al. 2016). A limitation of using uncorrected FA as a measure of diffusion and neurodegeneration is that free water in the extracellular space can lead to spurious FA aliasing of extracellular and intracellular/axonal water signals and as a result, true FA changes are masked (Bergamino et al. 2016). However, it should be pointed out that the free water index also has limitations in terms of interpretability, which requires further experimentation beyond that conducted in the present work. The volume of the extracellular space, its viscosity, intermembrane gaps, and other factors such as composition and tortuosity of the extracellular matrix might affect diffusion relative to compartments permissive of free unhindered diffusion (Rusakov and Kullmann 1998; Chen and Nicholson 2000; Vorisek et al. 2002). It is unclear whether increased Ifn-γ expression directly modifies one or all of these extracellular factors. Given that Ifn-γ expression triggers the production of immune signaling proteins that alter vascular permeability (such as Timp1 and SerpinG1), astroglial proliferation and lymphocyte rolling (in response to chemokines such as Ccl8 and Cxcl10), axonal/dendritic deterioration, dystrophic calcinosis and cellular death, it is possible that Ifn-γ expression can potentially alter the extracellular volume contributing to the free water index through multiple mechanisms.

We should note several important limitations of the present study. The enlargement of cerebral ventricles in 8-month Ifn-γ mice can likely have an influence on the free water values for surrounding ROIs through partial volume averaging. We have previously reported cerebroventricular enlargement in mice overexpressing inflammatory interleukin-6 (Colon-Perez et al. 2019). This would make sense given the large free water values obtained from the areas affected by Ifn-γ, which were in the range of 0.4–0.8 similar to CSF regions. Another possibility is infiltration of CSF into tissue parenchymal spaces during a severe chronic inflammatory response. Because these changes were not observed in *Ifngr1*$^{-/-}$ and *Stat1*$^{-/-}$ mice, it is concluded here that these alterations potentially involving CSF water/partial volume averaging is still important as a potential marker of the effects of inflammatory signaling on tissue microstructure. Another limitation is that we did not offer direct experimental evidence that the free water imaging method is superior to other conventional (clinical) methods in detecting signs of neuroinflammation or neurodegeneration. We did not include comparisons with other methods, such as fluid-attenuated inversion recovery. This will be considered in future work.

Relevant to the present work are also two important caveats of the bi-tensor fitting using the regularization method that were previously summarized by Pasternak and colleagues (Pasternak et al. 2009). One of the main concerns that could arise is the effect of water exchange between compartments. The tensor approach does not take this into account and, therefore, in the present Ifn-γ mouse model, there may be biasing of free water values (and FA) as a result of conditions that alter cellular or structural permeability, as might occur in areas near cerebroventricles in the present study. Another potential pitfall relates to restrictions in the use of the bi-tensor model in a single-shell diffusion sequence which omits more complicated (non-Gaussian) aspects of diffusion attenuation. The non-Gaussian diffusion decay at larger shells perhaps more appropriately incorporate extracellular cellular presence in immune active conditions.

In conclusion, the present data suggest that free water index to map extracellular volume should be considered in further experimentation to understand early 'trigger' factors that lead to neurodegenerative cell loss or increases in inflammatory signaling. Artificially elevating brain levels of Ifn-γ promotes a chronic inflammatory environment, which with age causes significant loss of dopaminergic neurons (Chakrabarty et al. 2011). This neurodegenerative phenotype induced through inflammatory signaling was detected in WT mice as early as 1–3 months. In addition, the prevention of Ifn-γ effects on brain free water changes in *Ifngr1*$^{-/-}$ and *Stat1*$^{-/-}$ mice hint at the potential specificity of the changes in free water index induced by Ifn-γ.

Acknowledgements This work was supported by the National Institutes of Health (P50AG047266, R01NS052318, R01NS075012, T32NS082168, P50NS091856, 1R01AG055798). The authors thank the Advanced Magnetic Resonance Imaging and Spectroscopy (AMRIS) facility and National High Magnetic Field Laboratory

(NHMFL) for their continued support (National Science Foundation Cooperative Agreement No. DMR-1157490 and the State of Florida).

Author contributions MF planned the experiments, imaged mice, analyzed data, and wrote the manuscript. PC planned the experiments, wrote the manuscript, injected neonatal mice, performed immunohistochemistry and analysis. CCD injected neonatal mice and performed immunohistochemistry. PDP planned experiments, imaged mice, contributed to manuscript writing and editing. EO made custom modifications to free water algorithm for mouse brain image analysis. LMCP carried out the free water correction processing on MATLAB, contributed to manuscript writing and editing. DEV made custom modifications to free water algorithm for mouse brain image analysis, provided overall support and contributed to manuscript writing and editing. TEG planned experiments, provided overall support and contributed to manuscript writing and editing.

Funding This work was supported by the National Institutes of Health (P50AG047266, R01NS052318, R01NS075012, T32NS082168, P50NS091856, 1R01AG055798).

Compliance with ethical standards

Conflict of interest Authors declare that they have no competing interests.

Ethics approval All procedures received prior approval from the Institutional Animal Care and Use Committee of the University of Florida and follow all applicable NIH guidelines.

References

Albi A, Pasternak O, Minati L, Marizzoni M, Bartres-Faz D, Bargallo N, Bosch B, Rossini PM, Marra C, Muller B, Fiedler U, Wiltfang J, Roccatagliata L, Picco A, Nobili FM, Blin O, Sein J, Ranjeva JP, Didic M, Bombois S, Lopes R, Bordet R, Gros-Dagnac H, Payoux P, Zoccatelli G, Alessandrini F, Beltramello A, Ferretti A, Caulo M, Aiello M, Cavaliere C, Soricelli A, Parnetti L, Tarducci R, Floridi P, Tsolaki M, Constantinidis M, Drevelegas A, Frisoni G, Jovicich J, PharmaCog C (2017) Free water elimination improves test-retest reproducibility of diffusion tensor imaging indices in the brain: a longitudinal multisite study of healthy elderly subjects. Hum Brain Mapp 38(1):12–26. https://doi.org/10.1002/hbm.23350

Assaf Y, Basser PJ (2005) Composite hindered and restricted model of diffusion (CHARMED) MR imaging of the human brain. Neuroimage 27(1):48–58. https://doi.org/10.1016/j.neuroimage.2005.03.042

Ayers JI, Fromholt S, Sinyavskaya O, Siemienski Z, Rosario AM, Li A, Crosby KW, Cruz PE, DiNunno NM, Janus C, Ceballos-Diaz C, Borchelt DR, Golde TE, Chakrabarty P, Levites Y (2015) Widespread and efficient transduction of spinal cord and brain following neonatal AAV injection and potential disease modifying effect in ALS mice. Mol Ther 23(1):53–62. https://doi.org/10.1038/mt.2014.180

Behrens TE, Woolrich MW, Jenkinson M, Johansen-Berg H, Nunes RG, Clare S, Matthews PM, Brady JM, Smith SM (2003) Characterization and propagation of uncertainty in diffusion-weighted MR imaging. Magn Reson Med 50(5):1077–1088. https://doi.org/10.1002/mrm.10609

Bergamino M, Pasternak O, Farmer M, Shenton ME, Hamilton JP (2016) Applying a free-water correction to diffusion imaging data uncovers stress-related neural pathology in depression. Neuroimage Clin 10:336–342. https://doi.org/10.1016/j.nicl.2015.11.020

Boska MD, Hasan KM, Kibuule D, Banerjee R, McIntyre E, Nelson JA, Hahn T, Gendelman HE, Mosley RL (2007) Quantitative diffusion tensor imaging detects dopaminergic neuronal degeneration in a murine model of Parkinson's disease. Neurobiol Dis 26(3):590–596. https://doi.org/10.1016/j.nbd.2007.02.010

Burciu RG, Ofori E, Archer DB, Wu SS, Pasternak O, McFarland NR, Okun MS, Vaillancourt DE (2017) Progression marker of Parkinson's disease: a 4-year multi-site imaging study. Brain 140(8):2183–2192. https://doi.org/10.1093/brain/awx146

Castano A, Herrera AJ, Cano J, Machado A (2002) The degenerative effect of a single intranigral injection of LPS on the dopaminergic system is prevented by dexamethasone, and not mimicked by rh-TNF-alpha, IL-1beta and IFN-gamma. J Neurochem 81(1):150–157

Chakrabarty P, Ceballos-Diaz C, Lin WL, Beccard A, Jansen-West K, McFarland NR, Janus C, Dickson D, Das P, Golde TE (2011) Interferon-gamma induces progressive nigrostriatal degeneration and basal ganglia calcification. Nat Neurosci 14(6):694–696. https://doi.org/10.1038/nn.2829

Chen G, Adleman NE, Saad ZS, Leibenluft E, Cox RW (2014) Applications of multivariate modeling to neuroimaging group analysis: a comprehensive alternative to univariate general linear model. Neuroimage 99:571–588. https://doi.org/10.1016/j.neuroimage.2014.06.027

Chen KC, Nicholson C (2000) Spatial buffering of potassium ions in brain extracellular space. Biophys J 78(6):2776–2797. https://doi.org/10.1016/S0006-3495(00)76822-6

Colon-Perez LM, Ibanez KR, Suarez M, Torroella K, Acuna K, Ofori E, Levites Y, Vaillancourt DE, Golde TE, Chakrabarty P, Febo M (2019) Neurite orientation dispersion and density imaging reveals white matter and hippocampal microstructure changes produced by Interleukin-6 in the TgCRND8 mouse model of amyloidosis. Neuroimage 202:116138. https://doi.org/10.1016/j.neuroimage.2019.116138

Cox RW (1996) AFNI: software for analysis and visualization of functional magnetic resonance neuroimages. Comput Biomed Res 29(3):162–173

DeSimone JC, Febo M, Shukla P, Ofori E, Colon-Perez LM, Li Y, Vaillancourt DE (2016) In vivo imaging reveals impaired connectivity across cortical and subcortical networks in a mouse model of DYT1 dystonia. Neurobiol Dis 95:35–45. https://doi.org/10.1016/j.nbd.2016.07.005

DeSimone JC, Pappas SS, Febo M, Burciu RG, Shukla P, Colon-Perez LM, Dauer WT, Vaillancourt DE (2017) Forebrain knock-out of torsinA reduces striatal free-water and impairs whole-brain functional connectivity in a symptomatic mouse model of DYT1 dystonia. Neurobiol Dis 106:124–132. https://doi.org/10.1016/j.nbd.2017.06.015

Durbin JE, Hackenmiller R, Simon MC, Levy DE (1996) Targeted disruption of the mouse Stat1 gene results in compromised innate immunity to viral disease. Cell 84(3):443–450

Febo M, Foster TC (2016) Preclinical magnetic resonance imaging and spectroscopy studies of memory, aging, and cognitive decline. Front Aging Neurosci 8:158. https://doi.org/10.3389/fnagi.2016.00158

Ferris CF, Kulkarni P, Toddes S, Yee J, Kenkel W, Nedelman M (2014) Studies on the Q175 knock-in model of Huntington's disease using functional imaging in awake mice: evidence of olfactory dysfunction. Front Neurol 5:94. https://doi.org/10.3389/fneur.2014.00094

Hoy AR, Ly M, Carlsson CM, Okonkwo OC, Zetterberg H, Blennow K, Sager MA, Asthana S, Johnson SC, Alexander AL, Bendlin BB (2017) Microstructural white matter alterations in preclinical Alzheimer's disease detected using free water elimination

diffusion tensor imaging. PLoS One 12(3):e0173982. https://doi.org/10.1371/journal.pone.0173982

Huang S, Hendriks W, Althage A, Hemmi S, Bluethmann H, Kamijo R, Vilcek J, Zinkernagel RM, Aguet M (1993) Immune response in mice that lack the interferon-gamma receptor. Science (New York, NY) 259(5102):1742–1745

Jenkinson M, Bannister P, Brady M, Smith S (2002) Improved optimization for the robust and accurate linear registration and motion correction of brain images. Neuroimage 17(2):825–841

Ji F, Pasternak O, Liu S, Loke YM, Choo BL, Hilal S, Xu X, Ikram MK, Venketasubramanian N, Chen CL, Zhou J (2017) Distinct white matter microstructural abnormalities and extracellular water increases relate to cognitive impairment in Alzheimer's disease with and without cerebrovascular disease. Alzheimers Res Ther 9(1):63. https://doi.org/10.1186/s13195-017-0292-4

Khairnar A, Ruda-Kucerova J, Drazanova E, Szabo N, Latta P, Arab A, Hutter-Paier B, Havas D, Windisch M, Sulcova A, Starcuk Z Jr, Kiraly A, Rektorova I (2015) Late-stage alpha-synuclein accumulation in TNWT-61 mouse model of Parkinson's disease detected by diffusion kurtosis imaging. J Neurochem. https://doi.org/10.1111/jnc.13500

Liscovitch N, French L (2014) Differential co-expression between alpha-Synuclein and IFN-gamma signaling genes across development and in Parkinson's disease. PLoS One 9(12):e115029. https://doi.org/10.1371/journal.pone.0115029

Maier-Hein KH, Westin CF, Shenton ME, Weiner MW, Raj A, Thomann P, Kikinis R, Stieltjes B, Pasternak O (2015) Widespread white matter degeneration preceding the onset of dementia. Alzheimers Dement 11(5):485–493. https://doi.org/10.1016/j.jalz.2014.04.518

Metzler-Baddeley C, O'Sullivan MJ, Bells S, Pasternak O, Jones DK (2012) How and how not to correct for CSF-contamination in diffusion MRI. Neuroimage 59(2):1394–1403. https://doi.org/10.1016/j.neuroimage.2011.08.043

Ofori E, Krismer F, Burciu RG, Pasternak O, McCracken JL, Lewis MM, Du G, McFarland NR, Okun MS, Poewe W, Mueller C, Gizewski ER, Schocke M, Kremser C, Li H, Huang X, Seppi K, Vaillancourt DE (2017) Free water improves detection of changes in the substantia nigra in parkinsonism: a multisite study. Mov Disord 32(10):1457–1464. https://doi.org/10.1002/mds.27100

Ofori E, Pasternak O, Planetta PJ, Burciu R, Snyder A, Febo M, Golde TE, Okun MS, Vaillancourt DE (2015a) Increased free water in the substantia nigra of Parkinson's disease: a single-site and multi-site study. Neurobiol Aging 36(2):1097–1104. https://doi.org/10.1016/j.neurobiolaging.2014.10.029

Ofori E, Pasternak O, Planetta PJ, Li H, Burciu RG, Snyder AF, Lai S, Okun MS, Vaillancourt DE (2015b) Longitudinal changes in free-water within the substantia nigra of Parkinson's disease. Brain 138(Pt 8):2322–2331. https://doi.org/10.1093/brain/awv136

Pasternak O, Koerte IK, Bouix S, Fredman E, Sasaki T, Mayinger M, Helmer KG, Johnson AM, Holmes JD, Forwell LA, Skopelja EN, Shenton ME, Echlin PS (2014) Hockey Concussion Education Project, Part 2 Microstructural white matter alterations in acutely concussed ice hockey players: a longitudinal free-water MRI study. J Neurosurg 120(4):873–881. https://doi.org/10.3171/2013.12.JNS132090

Pasternak O, Kubicki M, Shenton ME (2016) In vivo imaging of neuroinflammation in schizophrenia. Schizophr Res 173(3):200–212. https://doi.org/10.1016/j.schres.2015.05.034

Pasternak O, Sochen N, Gur Y, Intrator N, Assaf Y (2009) Free water elimination and mapping from diffusion MRI. Magn Reson Med 62(3):717–730. https://doi.org/10.1002/mrm.22055

Pasternak O, Westin CF, Bouix S, Seidman LJ, Goldstein JM, Woo TU, Petryshen TL, Mesholam-Gately RI, McCarley RW, Kikinis R, Shenton ME, Kubicki M (2012) Excessive extracellular volume reveals a neurodegenerative pattern in schizophrenia onset. J Neurosci 32(48):17365–17372. https://doi.org/10.1523/JNEUROSCI.2904-12.2012

Planetta PJ, Ofori E, Pasternak O, Burciu RG, Shukla P, DeSimone JC, Okun MS, McFarland NR, Vaillancourt DE (2016) Free-water imaging in Parkinson's disease and atypical parkinsonism. Brain 139(Pt 2):495–508. https://doi.org/10.1093/brain/awv361

Rusakov DA, Kullmann DM (1998) A tortuous and viscous route to understanding diffusion in the brain. Trends Neurosci 21(11):469–470

Sahara N, Perez PD, Lin WL, Dickson DW, Ren Y, Zeng H, Lewis J, Febo M (2014) Age-related decline in white matter integrity in a mouse model of tauopathy: an in vivo diffusion tensor magnetic resonance imaging study. Neurobiol Aging 35(6):1364–1374. https://doi.org/10.1016/j.neurobiolaging.2013.12.009

Saxena S, Caroni P (2011) Selective neuronal vulnerability in neurodegenerative diseases: from stressor thresholds to degeneration. Neuron 71(1):35–48. https://doi.org/10.1016/j.neuron.2011.06.031

Schwartz M, Deczkowska A (2016) Neurological disease as a failure of brain-immune crosstalk: the multiple faces of neuroinflammation. Trends Immunol 37(10):668–679. https://doi.org/10.1016/j.it.2016.08.001

Smith SM, Jenkinson M, Woolrich MW, Beckmann CF, Behrens TE, Johansen-Berg H, Bannister PR, De Luca M, Drobnjak I, Flitney DE, Niazy RK, Saunders J, Vickers J, Zhang Y, De Stefano N, Brady JM, Matthews PM (2004) Advances in functional and structural MR image analysis and implementation as FSL. Neuroimage 23(Suppl 1):S208–219. https://doi.org/10.1016/j.neuroimage.2004.07.051

Strickland MR, Koller EJ, Deng DZ, Ceballos-Diaz C, Golde TE, Chakrabarty P (2017) Ifngr1 and Stat1 mediated canonical Ifn-gamma signaling drives nigrostriatal degeneration. Neurobiol Dis 110:133–141. https://doi.org/10.1016/j.nbd.2017.11.007

Vorisek I, Hajek M, Tintera J, Nicolay K, Sykova E (2002) Water ADC, extracellular space volume, and tortuosity in the rat cortex after traumatic injury. Magn Reson Med 48(6):994–1003. https://doi.org/10.1002/mrm.10305

Wyss-Coray T (2016) Ageing, neurodegeneration and brain rejuvenation. Nature 539(7628):180–186. https://doi.org/10.1038/nature20411

Yushkevich PA, Piven J, Hazlett HC, Smith RG, Ho S, Gee JC, Gerig G (2006) User-guided 3D active contour segmentation of anatomical structures: significantly improved efficiency and reliability. Neuroimage 31(3):1116–1128. https://doi.org/10.1016/j.neuroimage.2006.01.015

Zaitout Z, Romanowski C, Karunasaagarar K, Connolly D, Batty R (2014) A review of pathologies associated with high T1W signal intensity in the basal ganglia on magnetic resonance imaging. Pol J Radiol 79:126–130. https://doi.org/10.12659/PJR.890043

Zhang H, Schneider T, Wheeler-Kingshott CA, Alexander DC (2012) NODDI: practical in vivo neurite orientation dispersion and density imaging of the human brain. Neuroimage 61(4):1000–1016. https://doi.org/10.1016/j.neuroimage.2012.03.072